Biosensors and Bioelectronics 38 (2012) 19–26

Contents lists available at SciVerse ScienceDirect

Biosensors and Bioelectronics

journal homepage: www.elsevier.com/locate/bios

A 3D localized surface plasmon resonance biosensor for the study of trivalent arsenic binding to the ArsA ATPase

Chang Liu [a], Vittoria Balsamo [b], Dali Sun [a], Melodie Naja [d], Xuemei Wang [e], Barry Rosen [c], Chen-Zhong Li [a,*]

[a] Nanobioengineering/Nanobioelectronics Laboratory, Department of Biomedical Engineering, Florida International University, 10555 W Flagler Street, Miami, FL 33174, USA
[b] Departamento de Ciencia de los Materiales, Universidad Simon Bolivar, Apartado 89000, Caracas1080 A, Venezuela
[c] Department of Cellular Biology and Pharmacology, Herbert Wertheim College of Medicine, Florida International University, 11200 S.W. 8th Street, AHC 2, Miami, FL 33199, USA
[d] Everglades Foundation, 18001 Old Cutler Road, Palmetto Bay, FL 33157, USA
[e] State Key Lab of Bioelectronics (Chien-Shiung Wu Laboratory), Southeast University, No. 2 Sipailou, Nanjing 210096, China

ARTICLE INFO

Article history:
Received 11 February 2012
Received in revised form
12 April 2012
Accepted 13 April 2012
Available online 26 April 2012

Keywords:
Localized surface plasmon resonance
Optical biosensor
Arsenic
Binding kinetics
Nanoparticle
3-D polymer

ABSTRACT

A self-assembled 3D hydrogel–nanoparticle composite integrated surface plasmon resonance (SPR) sensor is reported here. The novel assembled substrate was developed by means of a surface mediated radical co-polymerization process to obtain a highly sensitive hydrogel-based thin film that possesses specific binding sites for target analytes. Initially, amino group modified gold nanoparticles (AuNPs) were covalently linked to acrylic acid monomer. Following this, N-isopropylacrylamide (NIPAAm) and AuNPs linked acrylic acid (AAc) monomers were randomly co-polymerized by the "grafting from" method in the presence of initiator and crosslinker onto the sensing surface. Surface charecterization techniques were utilized to evaluate the thickness and composition of the hydrogel-nanoparticle film. The sensing platform was employed to study the binding kinetics and conformational changes of the ArsA ATPase as a consequence of binding trivalent arsenicals under a variety of conditions. ArsA, the catalytic subunit of the ArsAB arsenite (As(III)) translocating ATPase, is one of the five proteins encoded by the arsenical resistance (*ars*) operon of plasmid R773 in cells of *Escherichia coli*, that confers resistance to trivalent and pentavalent salts of the metalloid arsenic. SPR measurements indicate that the 3D hydrogel-nanoparticle coated sensors exhibited a higher sensitivity than that of the 2D AuNPs decorated sensors. Binding of As(III) to ArsA is greatly facilitated by the presence of magnesium ion and ATP.

1. Introduction

Surface plasmon resonance has brought a revolutionary change to *in vitro* study of biological and biochemical processes due to its ability to measure extremely small changes in surface refractive index (RI), binding equilibrium and kinetics (Turner, 2000; Lee et al., 2006; Natsume et al., 2000; Quinn et al., 2000; Gao et al., 2006; Cooper, 2003). Strategies based on plasmonic nanoparticles have been employed to enhance the sensitivity for a variety of applications, such as diagnosis of diseases, environmental analysis, food safety, and chemical threat detection (Shan et al., 2010; Ali Syed et al., 2011). Theoretically, SPR can be induced only in free electron metals, e.g., Au, Ag and Cu, due to the interaction of surface electrons with the electromagnetic wave and the contribution from the interband transition of the d-shell electrons (Beyene et al., 2010; Raether, 1988). At the end of the 1990s, several research groups had begun exploring schemes for the development of localized surface plasmon resonance (LSPR) biosensors using noble metal nanoparticles because of the extremely sensitive nature of their electron-rich surfaces to the surrounding environment. Based on the Mie theory, when an electromagnetic wave is directed to the metallic nanoparticle, an induced oscillation of free electrons occurs at the surface, resulting in a characteristic extinction spectrum that depends on the type of metal, the size and shape of the nanoparticles, interparticle distance and most importantly, the RI of the surrounding medium (Jung et al., 1998; Link and El-Sayed, 1999; Kreibig and Vollmer, 1995). Compositional and conformational changes within the surrounding dielectric medium near a nanoparticle could therefore be detected as shifts in the extinction spectrum. LSPR spectroscopy operates in a manner that is analogous to SPR to induce the extinction spectrum, however, the electromagnetic field of LSPR decays within a much smaller length than in SPR, which gives significant rise to the sensitivity of LSPR sensors. In 2008, Miura's group demonstrated a prototype field portable LSPR system using monoclonal trinitrotoluene (TNT) antibody modified AuNPs for detection of TNT (Kawaguchi et al., 2008). They achieved a detectable range of 10 ppt to 100 ppb, which is four-fold more sensitive than that in the absence of AuNPs.

* Corresponding author. Tel.: +305 348 0120; fax: +305 348 6954.
E-mail address: licz@fiu.edu (C.-Z. Li).

0956-5663/$ - see front matter © 2012 Elsevier B.V. All rights reserved.
http://dx.doi.org/10.1016/j.bios.2012.04.026

Using a similar principle, Kim's group recently constructed an LSPR biosensor based on subwavelength 1D and 2D gold nanoarrays built on a thin gold film for the detection of avian influenza DNA hybridization (Kim et al., 2010). Their results showed that 1D nanogratings exhibited four-fold amplification of the SPR signal, and 2D nanohole arrays exhibited a 2.5-fold increase in amplification. Although such technologies have successfully demonstrated high detection sensitivity in the range of picomolar of analytes, small molecules such as heavy metal ions have had difficulty being measured using this current setup.

The fabrication of the metallic nanostructure on the LSPR sensing layer is traditionally performed by "2D" methods. DebRoy's group immobilized polyclonal antibodies for *Escherichia coli (E. coli)* O157:H7 using biotin–neutravidin binding to detect *E. coli* O157:H7 spiked in pasteurized milk (skim-milk), apple juice, and ground beef extract (Waswa et al., 2007). They also functionalized a SPR gold chip with carboxymethylated dextran layer followed by Protein A to immobilize polyclonal antibodies against *E. coli* or *Salmonella Enteritidis* (Waswa et al., 2006). In these cases, low concentration targets in the sample were difficult to detect because of the limited interaction time with the sensing surface due to continuous flow. Signal amplification is a common strategy for detection of low concentrations of target molecules. Cheng's research group recently reported a novel SPR signal amplification strategy based on *in situ* surface-initiated atom transfer radical polymerization (Liu et al., 2010), in which a polymer was used as a label for small molecules. Another feasible strategy is the functionalization of the SPR sensor chip with an absorbtive coating in addition to using bare nanoscale noble metal structures for amplifying the sensor response. Radical copolymers would be ideal materials for this purpose due to their high capacity for absorbing the analyte via a swelling-shrinking process upon interacting with a water based buffer, enabling the sensing surface to capture larger amount of analyte (Zhang et al., 2002). This property allows interparticle distance tuning. Poly (*N*-isopropylacrylamide) (PNIPAAm) is a promising material that can satisfy these requirements (Chang et al., 2009; Lindqvist et al., 2008). Furthermore, copolymers obtained from the combination of polymers may result in even more sensing applications, as polymers with different functional groups allow the modulation of the material's final properties for recognizing different analytes. Finally, radical copolymers prevent non-specific binding to the remaining free gold surface in between the probes. This method is comparable to the conventional immunoassay approach in which the surface is masked with a high concentration of a non-specific protein such as bovine serum albumin or denatured casein (Ehrentreich-Forster et al., 2003).

Arsenic (As) is one of the most common toxic elements in the environment and is introduced by both geochemical and anthropogenic sources. Exposure to this metalloid leads to cancer, cardiovascular and peripheral vascular diseases, diabetes and neurological disease (Abernathy et al., 2003). The field of arsenic detoxification has been studied for many decades (Bhattacharjee and Rosen, 2007). Nearly every organism, from bacteria to humans, has an arsenic detoxifying system. In bacteria and archaea, the genes for arsenic resistance are usually found in arsenical resistance (*ars*) operons. One such operon, the *ars* operon of plasmid R773, produces resistance to trivalent and pentavalent salts of the metalloids arsenic and antimony in cells of *E. coli* catalyzed by an ATP-coupled $As(OH)_3$ extrusion pump (Chen and Rosen, 1997). The operon has five genes, *arsRDABC* (San Francisco et al., 1990). Among them, ArsR is a trans-acting repressor protein that homeostatically regulates the levels of *ars* transcription (Wu and Rosen, 1993). ArsD is an As(III) chaperone that binds and transfers cytosolic arsenite to ArsA, an As(III)-activated ATPase (Lin et al., 2006). Together ArsA and ArsB, a transmembrane arsenite antiporter, form the ATP-driven ArsAB $As(OH)_3$ extrusion pump (Chen et al., 1986). In 2006, Tao's group reported the first application of SPR sensing for arsenic detection in groundwater (Forzani et al., 2007). However, there are no reports that utilize this technique for kinetics study on arsenic transportation and detoxification to date.

In this study, we integrated *in situ* radical copolymerization and AuNPs to construct a novel LSPR sensing system. By growing 3D AuNPs-doped PNIPAAm-*co*-PAAc hydrogel-based coating on the gold sensing surface, we observed a 6.8-fold enhancement of LSPR signal comparing to the traditional 2D AuNPs-decorated gold sensing surface. We applied this LSPR sensor to study the binding kinetics of the ArsA ATPase for As(III) in the presence of adenosine-5'-triphosphate and magnesium ion (MgATP) and ArsD. In previous studies, binding of As(III) by Ars proteins was performed by methods such as extended x-ray absorption fine structure (EXAFS) (Qin et al., 2007). EXAFS is a definitive method for analyzing metal ligands but lacks sensitivity and real-time analysis. In contrast, our 3D hydrogel based LSPR sensing strategy obtained direct, real-time binding kinetic information (Rich and Myszka, 2000). Thus, in addition to providing a means of amplifying the LSPR response, this work presents a novel approach to study the kinetic behavior of the arsenic extrusion pathway. Finally, the functionality of our novel 3D hydrogel-nanoparticle coating can be easily modified by changing or adjusting loading of monomers, it has potential to be broadly applied to sensing a range of biological analytes.

2. Experimental

2.1. Materials

Allylmercaptan, AAc, NIPAAm, N,N-methylenebisacrylamide (BIS) were purchased from Acros Organic (New Jersey), 2,2′azobisisobutyronitrile (AIBN) and diisopropylfluorophosphate (DIFP) were obtained from Sigma-Aldrich (St. Louis, MO). 11-mercaptoundecanoic acid (MUA) was purchased from Asemblon (Redmond, WA). Cystamine dihydrochloride was obtained from Spectrum (New Brunswick, NJ). 1-ethyl-3-(3-dimethylaminopropyl) carbodiimide hydrochloride (EDC), *N*-Hydroxysuccinamide (NHS) and hydrogen tetrachloroaurate ($HAuCl_4$) were obtained from Alfa Aesar (Ward Hill, MA). Trisodium citrate ($Na_3C_6H_5O_7$) and dimethyl sulfoxide (DMSO) were purchased from Fisher Scientific (Waltham, MA). All reagents and solvents were used as received.

2.2. Protein expression and purification

Cells bearing the indicated plasmids were grown in Lysogeny Broth (LB) medium overnight at 37 °C and then diluted 50-fold into 1 L of the same medium. Proteins were expressed by induction with 0.3 mM isopropyl-ß-D-thiogalactopyranoside at A_{600} of 0.6–0.8 for 3 h. ArsA with a six histidine tag at the C-terminus was purified from cells of strain BL21 (DE3) expressing pAlter-1-dAhB plasmid, as described (Zhou and Rosen, 1997). Cells were harvested by centrifugation and washed once with a buffer containing 50 mM 3-(N-morpholino)propanesulfonic acid (MOPS), pH 7.5, 0.5 M NaCl, 30 mM imidazole and 10 mM 2-mercaptoethanol (Buffer A). The cells were suspended in 5 mL of Buffer A per gram of wet cells and lysed by a single passage through a French press at 20,000 psi. DIFP was added at 2.5 mL/g wet cells immediately following French press. Unbroken cells and membranes were removed by centrifugation at 150,000 xg for 1 h at 4 °C. The supernatant was loaded to 10 mL Probond Ni-column (Invitrogen) pre-equilibrated with Buffer A. Unbound proteins were washed by 60 mL of buffer A, and ArsA was eluted with imidazole gradient generated by Buffer A and Buffer B (50 mM MOPS, pH 7.5, 0.5 M NaCl, 300 mM imidazole and

10 mM 2-mercaptoethanol), followed by addition of 0.25 mM Ethylenediaminetetraacetic acid (EDTA) and 5 mM Dithiothreitol (DTT) to each fraction. ArsA containing fractions were identified by sodium dodecyl sulfate polyacrylamide gel electrophoresis (SDS-PAGE), pooled, concentrated by Amicon Ultra-15 Centrifugal Filter Unit with Ultracel-10 membrane (Millipore), mixed with 10% glycerol, aliquoted and stored at −80 °C until use. ArsD and its derivatives with a six histidine tag at the N-terminus were purified similarly. Purified proteins were stored at −80 °C until use, and their concentrations were determined according to the method of Bradford (Bradford, 1976) or from the absorption at 280 nm (Gill and von Hippel, 1989).

2.3. Preparation of gold nanoparticles

Colloidal gold nanoparticles used in this study were prepared by citrate reduction of $HAuCl_4$ in aqueous solution (McFarland et al., 2004). The formation of gold nanoparticles can be observed by a change of color. Briefly, $HAuCl_4$ and sodium citrate solutions were filtered through a 22 μm microporous membrane filter prior to use. $HAuCl_4$ (40 mL, 1.0 mM) was then added to an Erlenmeyerflask (250 mL), vigorously stirred and brought to a boil on a hotplate. Following this, 3.5 mL of 1% trisodium citrate was added to the vortex of the boiling solution. 100 nm Au particles were formed 2 min after the addition of trisodium citrate and 15 nm AuNPs were obtained if the solution was stirred for an additional 10 min. A layer of absorbed citrate anions on the surface of the nanoparticles prevents aggregation. The particle size was determined by a ZEN3600 Zetasizer from Malvern Instruments, Inc. (Westborough, MA).

2.4. In-situ polymerization

A stock of amino group modified AuNPs was prepared by incubating bare AuNPs in 1 mM cystamine dihydrochloride solution for 12 h at 4 °C. Following this, 400 μmol AAc was added to the amino modified AuNPs and incubated under the presence of NHS/EDC for 30 min to form covalent linkage (pH=7.4). The resulting solution was then centrifuged at 7000 RCF for 10 min and the sediment was washed and resuspended with a same volume of DMSO for further use (not shown in Scheme 1). A gold

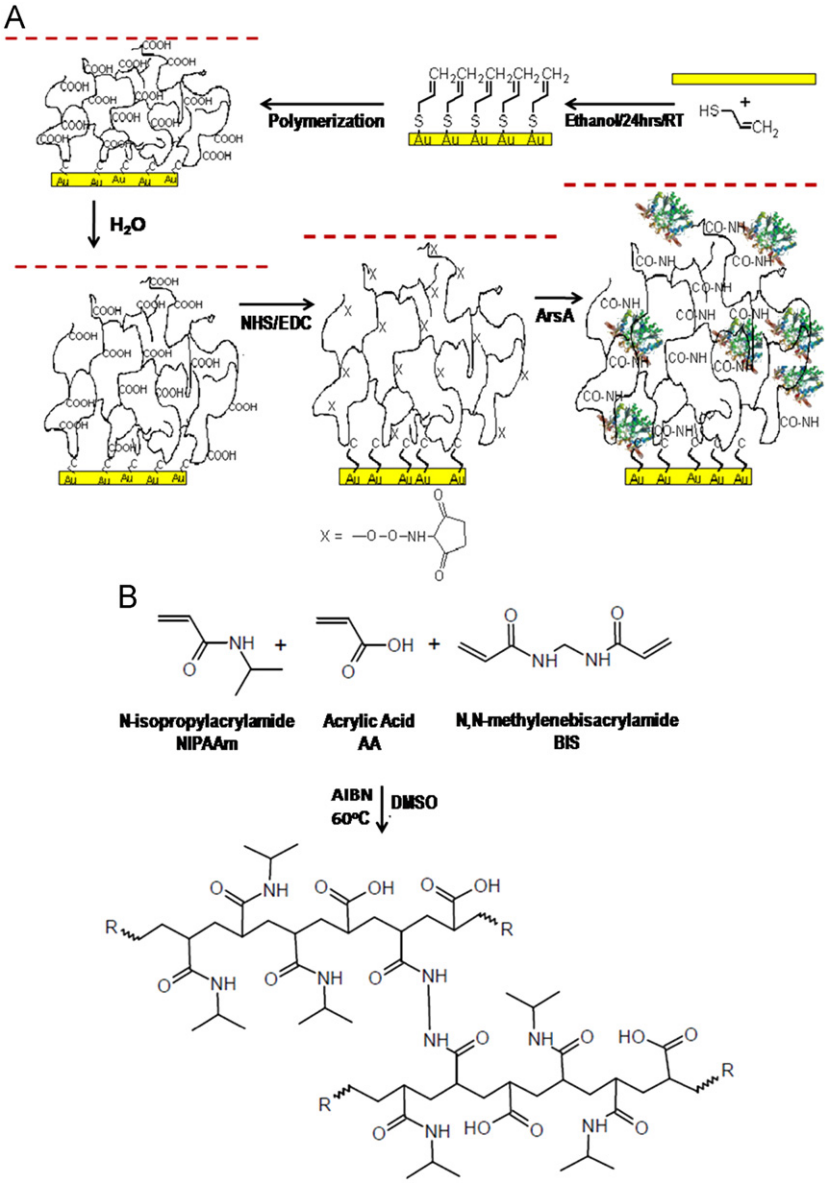

Scheme 1. (A) Cartoon representation of the swelling-shrinking process of the copolymer for LSPR signal amplification and immobilization of ArsA ATPase. (B) Structural illustration of the *in-situ* radical copolymerization of PNIPAAm-*co*-PAAc hydrogel.

SPR chip was cleaned using piranha solution for 2 min and rinsed with copious ethanol. The cleaned gold chip was incubated in a 10 mM allylmercaptan/ethanol solution afterward for 12 h at room temperature in the absence of light. Lastly, the chip was rinsed three times with ethanol and DMSO shortly prior to use to remove all the unbounded allylmercaptan residual. The *in situ* polymerization was carried out in the following manner: 5 mL DMSO containing 950 μmol of NIPA, 150 μmol of AuNPs linked AAc, 250 μmol of AAc, 58 μmol of crosslinking agent BIS and 805 μmol of AIBN as the initiator were first added along with the gold chip into a three-neck round bottom flask. The resulting solution was degassed by passage of a stream of nitrogen for a minimum of 20 min and then heated at 60 °C for 110 min in nitrogen environment (Scheme 1). After polymerization, the AuNPs doped PNIPAAm-*co*-PAAc polymer-coated gold chip was washed with DMSO, ethanol and water in order to remove any non-bonded copolymer and unreacted monomers. Finally, the chip was stored under vacuum to remove any water absorbed in the hydrogel before LSPR experiment. Control chips were also prepared by deposition of bare AuNPs on SPR chips and functionalized with carboxylic groups using MUA for characterization purposes.

2.5. Experimental setup and conditions

2.5.1. Surface characterization

Fourier transform infrared spectroscopy by attenuated total reflectance (ATR-FTIR) was carried out using a FTIR-4100 spectrometer (Easton, MD) with a maximum resolution of 0.9 cm. A Nanoscope 3A atomic force microscope (AFM) obtained from Veeco (Plainview, NY) was employed to measure the thickness of the polymer thin film on the gold chip. Briefly, a $10 \times 10\ \mu m^2$ area of the polymer layer was scratched and removed using a contact mode AFM cantilever (spring constant 0.2 Nm) under the load of 500 nN force. To determine the depth of the scratched area, the morphology of a $30 \times 30\ \mu m^2$ area covering the scratched area was imaged by AFM under a 25 N force load with a scanning speed of 2 Hz. A JSM6330F field emission scanning electron microscopy (SEM) from JEOL (Peabody, MA) was employed for observing the surface morphology and component of the LSPR sensing surface.

2.5.2. Preparation of LSPR measurement

A BI-2000 SPR instrument was purchased from Biosensing Instrument (Tempe, AZ). A gold SPR chip (20 mm × 20 mm × 1 mm), which is a BK7 glass slide coated with a 45 nm layer of gold over a 5 nm layer of chromium, was mounted on the upperface of the BK7 prism with the gold layer facing upward. A 3–5 μL drop of index matching fluid (World Precision Instruments, Inc., FL) was applied between the glass face of the chip and the prism with care so that no air bubbles were trapped at the interface. Following this, a biocompatible polydimethylsiloxane (PDMS) microfluidic injection chamber gasket with a 5 mm × 1.7 mm × 125 μm channel was clamped to the gold face of the chip. A dual syringe pump was attached to the injection chamber allowing both sample and reference buffer flow through the sensing surface. All buffers and solutions were degassed by vigorously stirring and purging with nitrogen before introduction into the injection system to avoid oxidation of ArsA ATPase and ArsD metallochaperone protein by air. Data collection and instrument control was performed using the Biosensing Instrument SPR Control Program running on a PC.

In the LSPR experiment, a 670 nm wavelength laser with a 72.2° incident angle was employed as the light source. The sensing surface was flushed by 50 mM MOPS buffer (pH 7.5) at a 150 μL/min flow rate until a stable SPR baseline was acquired. In general, a 100–150 mDeg SPR angle shift would be observed during this process due to the swelling of the PNIPAAm-*co*-PAAc hydrogel upon introduction of water based MOPS buffer. The MOPS flow rate was then reduced to 50 μL/min for optimized binding time and maintained during the whole LSPR measurement. All measurements were carried out in MPOS buffer environment unless otherwise stated.

In order to demonstrate the enhanced sensitivity by the polymer hydrogel thin layer as the immobilization and sensing material, as well as its suitability for binding kinetic study, ArsA ATPase was coupled to the carboxylic groups of AAc and the specific interaction of As(III) with the immobilized ArsA was observed by LSPR. Initially, carboxylic groups of the polymer layer were activated with a solution of EDC (75 mM) and NHS (15 mM) at an injection rate of 20 μL/min (denoted as X in Scheme 1). ArsA in MOPS with a concentration of 50 μg/mL was injected with a same rate and allowed to react with the activated polymer for 4 min to form a covalent linkage between the surface carboxylic groups and the ArsA amino-groups. This was followed by an addition of stepped concentration of As(III) to study the binding kinetics and capacity of the ArsA ATPase. Finally, the above experiment was repeated using control chipscoated only with AuNPs.

3. Results and discussion

3.1. Surface morphology and composition characterization

To verify the incorporation of NIPAAm and AAc monomeric units in the copolymer grown from the allylmercaptan-modified gold surface, ATR-FTIR spectra were taken from the polymer coated gold chip surface. As a result, Fig. 1 shows a region of the ATR-FTIR spectrum obtained, which confirms the presence of both NIPAm and AAc in the thin film. The main bands at located at 1651 and 1551 cm correspond to the carbonyl stretching of the amide group (amide I band) and to the N–H stretching of the

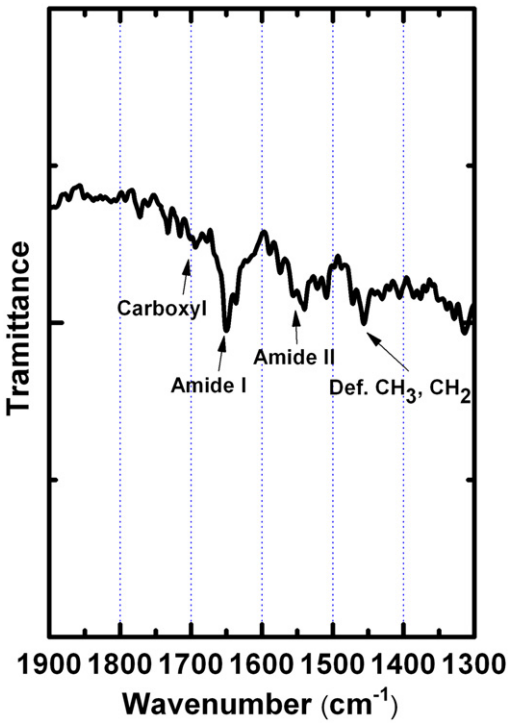

Fig. 1. FTIR-ATR spectrum of the 3D PNIPAAm-*co*-PAAc polymer matrix on the sensing surface.

secondary amide (amide II band), respectively. On the other hand, the appearance of a much less intense absorption band at 1716 cm, characteristic of the carboxyl group, indicates the incorporation of a minor acrylic acid fraction as expected. Besides, a band at 1460 cm is clearly observed, which can be attributed to the $-CH_3$ and $-CH_2-$ deformation of both monomeric units (Pan et al., 2001; Yang et al., 2004).

The thickness of the PNIPAAm-*co*-PAAc polymer layer under hydrated and dehydrated condition was determined by AFM using the aforementioned manner (Hirata et al., 2004). Fig. 2(A) shows the morphologies and line profiles of the scratched areas under both conditions, with the average thickness of each sample determined from the line profiles. The hydrated polymer layer displays a thickness of 40.6 ± 3 nm, whereas the dehydrated polymer layer exhibited a thickness of 10.1 ± 1 nm. Fig. 2(B) shows a SEM image in which AuNPs (bright dots) can be observed along the backbone of the polymer hydrogel, indicating that AuNPs were successfully embedded in the PNIPAAm-*co*-PAAc hydrogel by the linkage with AAc.

3.2. Optimization of ArsA immobilization conditions

The incubation time required for the binding reaction between ArsA and polymer matrix is a critical parameter that determines the performance of our kinetics sensor. Insufficient incubation time causes low coverage of ArsA on the surface and leads to lower sensitivity, whereas over-long incubation time may results in multiple layers of ArsA and leads to blockage of binding sites and lower efficiency. To optimize the time required for completeness of the covalent linking, 80 μg/mL ArsA solution was injected and past the PNIPAAm-*co*-PAAc modified gold sensing surface at various injection rates. LSPR angle shift was used to evaluate the surface coverage. As shown in Fig. 3(A), this study found that ArsA immobilization with a sample injection rate of 20 μL/min or slower exhibited a stable response demonstrating the complete interaction between ArsA and PNIPAAm-*co*-PAAc. Therefore, we employed optimized sample injection rate of 20 μL/min for further immobilization and analysis.

In order to evaluate the amount of ArsA ATPase immobilized on the surface of the 3D polymer matrix, we investigated the LSPR response to different concentrations of ArsA injections. Initially, 5 polymer modified LSPR chips were activated using 75 mM EDC and 15 mM NHS in MOPS buffer. Following activation, each activated sensor was employed to react with different concentrations of ArsA solution at an injection rate of 20 μL/min. The resulting LSPR response for each sensor was plotted against the corresponding concentration of ArsA as shown in Fig. 3(B). It is evident that the amount of ArsA ATPase bound to the sensing surface reaches a maximum at 50 μg/mL and remains constant at all concentration beyond. As a result, we employed 50 μg/mL as an optimum concentration for further binding study.

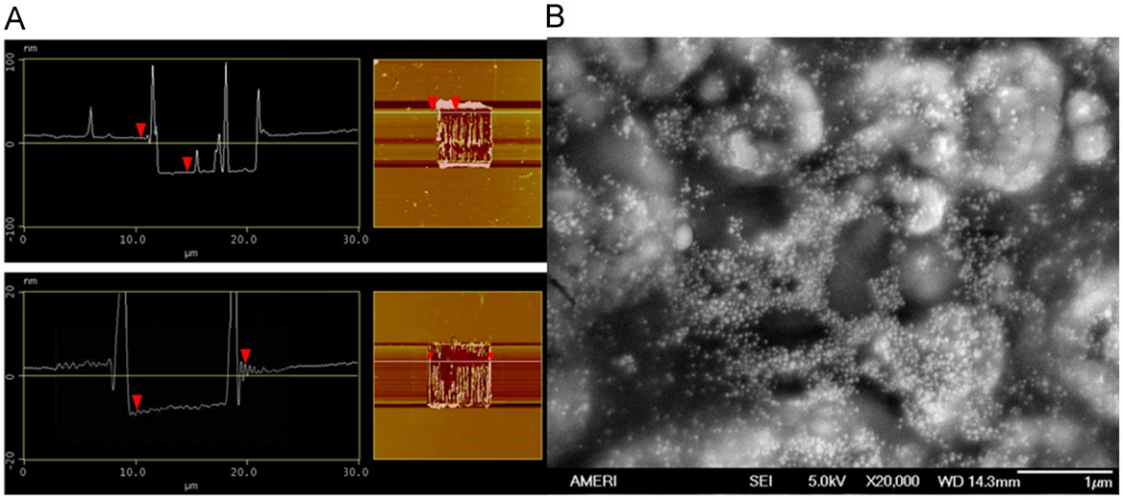

Fig. 2. (A) AFM images of the polymer matrices under hydrated (upper) and dehydrated (lower) conditions, indicating the swelling-shrinking process. (B) SEM image of the LSPR sensor coated with AuNPs doped hydrogel thin film.

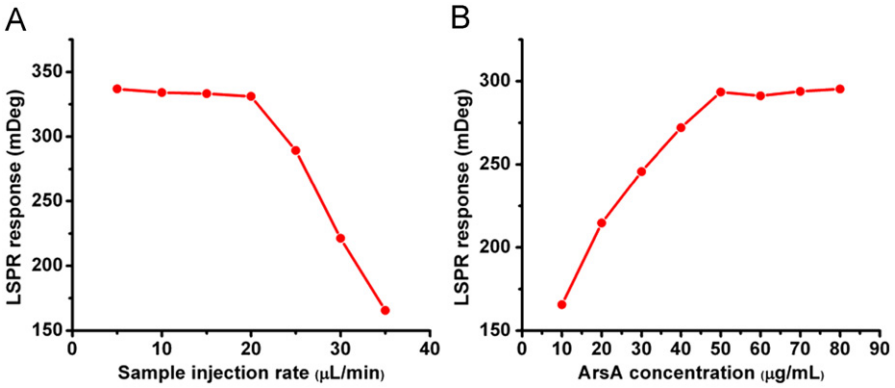

Fig. 3. Optimization of immobilization conditions. (A) ArsA immobilization on the 3D polymer coated surface with different injection rate (5, 10, 15, 20, 25, 30, 35 μL/min). Maximum SPR angle shift is plotted *versus* responding injection rate. (B) Different concentration of ArsA (10, 20, 30, 40, 50, 60, 70, 80 μg/mL) immobilization on the 3D polymer coated LSPR sensor with optimal injection rate (20 μL/min). Maximum SPR angle shift is plotted *versus* ArsA concentration.

3.3. ArsA and As(III) interaction

Sensitivity study was first performed with chips coated by AuNPs doped polymer layer. Prior to the binding test for each different concentrations of arsenite, ArsA was immobilized onto the activated carboxylic groups by the aforementioned protocol. Then, three different concentrations of arsenite (8 mM, 4 mM, 2 mM) were dosed separately with an injection rate of 20 μL/min. Fig. 4(a) shows the LSPR response to the injection of each arsenite sample. When the test solution was introduced at ~50 s, ~620 s and ~1100 s, a blue shift of 25.8 mDeg, 19.1 mDeg and 16.5 mDeg were observed corresponding to the introduction of 8 mM, 4 mM and 2 mM arsenite sample, respectively. The 2D AuNPs structure was not expected to induce as much LSPR enhancement as the 3D AuNPs doped polymer matrix according to our previous mentioned theory. Therefore, we repeated the binding experiment with chips decorated by 2D AuNPs structure. Fig. 4(b) indicates that a blue shift of 3.7 mDeg, 2.9 mDeg and 2.4 mDeg were recorded in response to the same concentration gradients of arsenite. As a result, the signal enhancement of the 3D polymer matrix was calculated to be about 6.8 fold. This increase can be attributed to the unique swelling-shrinking property of the PNIPAAm-*co*-PAAc hydrogel, yielding a greater capacity for ArsA immobilization than that of the 2D AuNPs chip (Scheme 1).

We expected larger enhancement from the 3D polymer matrix since the previous mentioned AFM measurements demonstrate that the thickness of the hydrated polymer is 40.615 nm, indicating an ideal capacity increase of 180 fold for ArsA (63 kDa, $a=73.34$, $b=75.64$, $c=223.42$ Å) compared to the ArsA monolayer formed on the 2D chip. One possible explanation for this discrepancy is the heterogeneous distribution of carboxylic groups during the random copolymer reaction resulting in a lack of available binding sites for ArsA. We also suspect that the injected ArsA bound to the surface of the polymer matrix has blocked the access of the unbound ArsA ATPase to binding sites inside the polymer matrix.

3.4. Kinetics study of ArsA–As(III) binding

ArsD is a metallochaperone that delivers As(III), as well as other trivalent metalloids, to the ArsA ATPase. Previous studies have shown that interaction with ArsD increases the affinity of ArsA for As(III), conferring resistance to environmental concentrations of arsenic (Yang et al., 2010). However, there is a lack of research on the binding affinity of ArsA for ArsD till now. Based on measurements on the effect of the As(III) chelator dimercaptosuccinic acid (DMSA) on the transfer reaction, it is suggested that As(III) transfer is directly channeling from one protein to the other, rather than dissociating from ArsD and reassociating with ArsA. Therefore, affinity study between ArsA and ArsD is essential to understanding the structure of ArsA–ArsD complex and improve understanding of the transfer reaction.

Initially, ArsA was immobilized to the activated carboxylic groups of the polymer as previously mentioned. Following this, 1% ethanolamine was injected to block the free carbonyl groups. ArsD metallochaperone (50 μg/mL) was then introduced to the flow chamber at 20 μL/min. For comparison, ArsD was substituted by bovine serum albumin (BSA) in the negative control experiment. Fig. S1 (supplementary materials) shows the LSPR sensorgram for the ArsA–ArsD interaction study. The binding between ArsA and ArsD (red) results in an angle shift of 356.2 mDeg, whereas the binding between ArsA and BSA (black) only results in an angle shift of 45.5 mDeg. Thus, it is evident that ArsA is able to specifically bind ArsD without the presence of As(III) and MgATP. This result is consistent with the direct transfer of As(III) in the ArsA–ArsD complex.

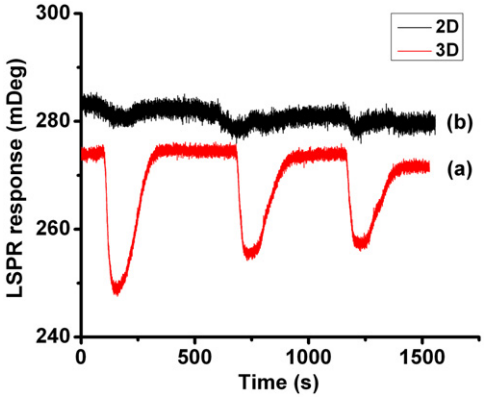

Fig. 4. SPR sensorgrams for the covalently immobilized ArsA interacting with As(III) obtained with (a) 3D AuNPs doped polymer coated sensor and (b) 2D AuNPs structure modified sensor.

3.5. Effects of ArsD and MgATP on ArsA–As(III) binding

We have previously shown that ArsD transfers As(III) and Sb(III) to ArsA in the presence of MgATP (Lin et al., 2007). Herein, binding kinetics of ArsA–As(III) interaction was compared using the 3D LSPR sensing platform under MgATP catalytic, ArsD promotion, and noncatalytic conditions.

ArsA was bound to the 3D LSPR sensing surface using the same manner. As(III) samples of 8 different concentrations (1–8 mM) were prepared in MOPS buffer. First, ArsA–As(III) binding kinetics was measured without catalysis as a control experiment. Samples with 1–8 mM As(III) were injected in 10 min interval between each other to allow for baseline stabilization. SPR angle shift — time curve (data not shown) was obtained for each sample in realtime. In the association phase, the reaction rate, dR/dt, can be described by the following equation:

$$\max\left(\frac{dR}{dt}\right) = k_a[\text{ArsA}][\text{As(III)}]$$

where R is the SPR signal at time t, k_a is the association rate constant which indicates the binding affinity between two reactants, [ArsA] and [As(III)] are the concentration of ArsA and As(III), respectively. The maximum value of (dR/dt) for each sample was determined by calculating the maximum slope of the association curve using Matlab. Linear fitting was utilized to obtain ka since [ArsA] is constant. Fig. 5(A) shows the ka calculated to be 1.07 M/min for noncatalytic ArsA–As(III) interaction. Based on the aforementioned study, interaction with ArsD increases the affinity of ArsA for As(III). Therefore, association rate constant was also measured for interaction under the presence of ArsD in the environmental buffer and ka was calculated to be 2.79 M/min as shown in Fig. 5(B). Furthermore, ArsA contains two nucleotide-binding sites (NBSs) and a binding site for arsenic, and crystallizes in the presence of As(III) and MgATP (Zhou et al., 2000). Based on these structural features, we tested association rate constant under the MgATP catalysis. Results show that the k_a was significantly raised to 16.09 M/min (Fig. 5(C)). By comparing these three sets of experiments, it is obvious that the binding efficiency is significantly raised under the presence of MgATP, indicating that the activity of the arsenic binding site is dependent on the binding status of the two NBSs for ATP. Based on the result, As(III) transfer occurs only under conditions where ArsA hydrolyzes ATP, suggesting that ArsD transfers As(III) to an ArsA conformation transiently formed during catalysis and not simply to the closed conformation that ArsA adopts when As(III) and MgATP are bound.

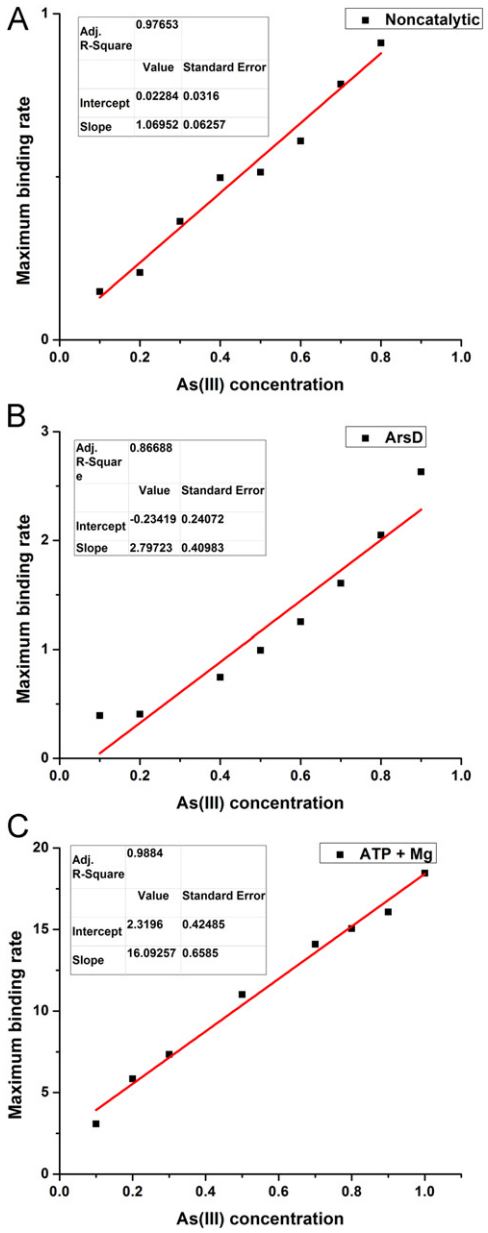

Fig. 5. Comparison of ArsA–As(III) association rate constant (slope) under the effect of different binding status. Figure showing: linear fitting curve of the relationship between maximum binding rate and As(III) concentration under (A) noncatalytic, (B) ArsD bounded and (C) MgATP catalyzing conditions of ArsA.

4. Conclusions

We have demonstrated the fabrication of AuNPs decorated 3D PNIPAAm-*co*-PAAc hydrogel modified LSPR sensors. Sensitivity enhancement of 7 fold was achieved for measurement of changes in bulk refractive index using LSPR spectroscopy, compared to the conventional 2D nanostructural LSPR sensor. Not only can the 3D hydrogel matrix act as a molecular sponge to increase the analyte absorbing capacity, but it also provides specificity, tunable size of porous structure and interparticle distance for different potential applications. Furthermore, we have demonstrated the ability of ArsA ATPase specifically bind ArsD metallochaperone without presence of As(III) and MgATP, thus proving the existence of the structure of ArsA–ArsD complex, which indicates direct channeling of As(III) from ArsD to ArsA. We also applied the 3D LSPR sensor to study the binding kinetics of the arsenic detoxifying systems found in *Escherichia coli*. Results indicates that transfer of As(III) from ArsD to ArsA is dependent on the binding and hydrolysis of MgATP.

Overall, this work presents a novel combination of a highly sorbtive polymer with AuNPs for enhanced sensitive LSPR spectroscopy. Real-time binding kinetics data were obtained by the LSPR sensor for further understanding of a biochemical process. The flexibility of this sensing platform to accommodate different ligands provides a practical strategy to detection and kinetic study of other biomolecules.

Acknowledgments

We thank FIU Graduate School Doctoral Evidence Acquisition Fellowship, AMERI (Advanced Material Engineering Research Institute, FIU) and DOD TATRC W81XWH-10-1-0732 for technical and financial support. This work has also been partially supported by U.S. Public Health Service Grant GM55425 to BPR, NIH R15 ES021079-01 to LiCZ, Everglades Foundation and Kauffman Foundations.

Appendix A. Supporting information

Supplementary data associated with this article can be found in the online version at http://dx.doi.org/10.1016/j.bios.2012.04.026.

References

Ali Syed, M., Bhatti, A.S., Li, C.-Z., Bokhari, H., 2011. American Journal of Biomedical Sciences 3, 253–257.
Abernathy, C.O., Thomas, D.J., Calderon, R.L., 2003. Journal of Nutritional 133, 1536–1538.
Beyene, H.T., Chakravadhanula, V.S.K., Hanisch, C., Elbahri, M., Strunskus, T., Zaporojtchenko, V., Kienle, L., Faupel, F., 2010. Journal of Materials Science 45, 5865–5871.
Bhattacharjee, H., Rosen, B.P., 2007. Arsenic metabolism in prokaryotic and eukaryotic microbes. In: Nies, D.H., Simon, S. (Eds.), In Molecular Microbiology of Heavy Metals. Springer-Verlag, Heidelberg/New York, pp. 371–406.
Bradford, M.M., 1976. Analytical Biochemistry 72, 248–254.
Chang, Y., Chen, W.Y., Yandi, W., Shih, Y.J., Chu, W.L., Liu, Y.L., Chu, C.W., Ruaan, R.C., Higuchi, A., 2009. Biomacromolecules 10, 2092–2100.
Chen, C.M., Misra, T.K., Silver, S., Rosen, B.P., 1986. Journal of Biological Chemistry 261, 15030–15038.
Chen, Y., Rosen, B.P., 1997. Journal of Biological Chemistry 272, 14257–14262.
Cooper, M.A., 2003. Analytical and Bioanalytical Chemistry 337, 834–842.
Ehrentreich-Forster, E., Scheller, F.W., Frieder, W., Bier, F.F., 2003. Biosensors and Bioelectronics 18, 375–380.
Forzani, E.S., Foley, K., Westerhoff, P., Tao, N.J., 2007. Sensors and Actuators B: Chemical 123, 82–88.
Gao, Y., Wolf, L.K., Georgiadis, R.M., 2006. Nucleic Acids Research 34. 3370–3337.
Gill, S.C., von Hippel, P.H., 1989. Analytical Biochemistry 182, 319–326.
Hirata, I., Okazaki, M., Iwata, H., 2004. Polymer 45, 5569–5578.
Jung, L.S., Campbell, C.T., Chinowsky, T.M., Mar, M.N., Yee, S.S., 1998. Langmuir 14, 5636–5648.
Kawaguchi, T., Shankaran, D.R., Kim, S.J., Matsumoto, K., Toko, K., Miura, N., 2008. Sensors and Actuators B: Chemical 133, 467–472.
Kim, S.A., Byun, K.M., Kim, K., Jang, S.M., Ma, K., Oh, Y., Kim, D., Kim, S.G., Shuler, M.L., Kim, S.J., 2010. Nanotechnology 21. 355503-35558.
Kreibig, U., Vollmer, M., 1995. Optical Properties of Metal Clusters. Springer-Verlag, Heidelberg, Germany 25.
Lee, H.J., Nedelkov, D., Corn, R.M., 2006. Analytical Chemistry 78, 6504–6510.
Lin, Y.F., Yang, J., Rosen, B.P., 2007. Journal of Biological Chemistry 282, 16783–16791.
Lin, Y.F., Walmsley, A.R., Rosen, B.P., 2006. Proceedings of the National academy of Sciences of the United States of America 103, 15617–15622.
Lindqvist, J., Nyström, D., Östmark, E., Antoni, P., Carlmark, A., Johansson, M., Hut, A., Malmström, E., 2008. Biomacromolecules 9, 2139–2145.
Link, S., El-Sayed, M.A., 1999. Journal of Physical Chemistry B 103, 8410–8426.
Liu, Y., Dong, Y., Jauw, J., Linman, M.J., Cheng, Q., 2010. Analytical Chemistry 82, 3679–3685.
McFarland, A.D., Haynes, C.L., Mirkin, C.A., Van Duyne, R.P., Godwin, H.A., 2004. Journal of Chemical Education 81, 544.
Natsume, T., Nakayame, H., Janssen, O., Isobe, T., Takio, K., Mikoshiba, K., 2000. Analytical Chemistry 72, 4193–4198.
Pan, Y.V., Wesley, R.A., Luginbuhl, R., 2001. Biomacromolecules 2, 32–36.

Qin, J., Fu, H.L., Ye, J., Bencze, K.Z., Stemmler, T.L., Rawlings, D.E., Rosen, B.P., 2007. Journal of Biological Chemistry 282, 34346–34355.
Quinn, J.G., O'Neill, S., Doyle, A., McAtammey, C., Diamond, D., MacCraith, B.D., O'Kennedy, R., 2000. Analytical Biochemistry 281, 135–143.
Raether, H., 1988. Surface Plasmons on Smooth and Rough Surfaces and on Gratings.
Rich, R.L., Myszka, D.G., 2000. Current Opinion in Biotechnology 11, 54–61.
San Francisco, M.J.D., Hope, C.L., Owolabi, J.B., Tisa, L.S., Rosen, B.P., 1990. Nucleic Acids Research 18, 619–624.
Shan, X., Huang, X., Foley, K.J., Zhang, P., Chen, K., Wang, S., Tao, N.J., 2010. Analytical Chemistry 82, 234–240.
Turner, A.P.F., 2000. Science 290, 1315–1317.
Waswa, J.W., Irudayaraj, J., DebRoy, C., 2007. LWT- Food Science and Technology 40, 187–192.
Waswa, J.W., DebRoy, C., Irudayaraj, J., 2006. Journal of Food Process Engineering 29, 373–385.
Wu, J.H., Rosen, B.P., 1993. Molecular Microbiology 8, 615–623.
Yang, J., Fang, Y., Bai, C., Hu, D., Zhang, Y., 2004. Chinese Science Bulletin 49, 2026–2032.
Yang, J., Rawat, S., Stemmler, T.L., Rosen, B.P., 2010. Biochemistry 49, 3658–3666.
Zhang, X.Z., Yang, Y.Y., Wang, F.J., Chung, T.S., 2002. Langmuir 18, 2013–2018.
Zhou, T., Rosen, B.P., 1997. Journal of Biological Chemistry 272, 19731–19737.
Zhou, T., Radaev, S., Rosen, B.P., Gatti, D.L., 2000. EMBO Journal 19, 4838–4845.